

# Multi-Scale Cell Decomposition for Path Planning using Restrictive Routing Potential Fields

Josue N. Rivera and Dengfeng Sun

**Abstract**—In burgeoning domains, like urban goods distribution, the advent of aerial cargo transportation necessitates the development of routing solutions that prioritize safety. This paper introduces Larp, a novel path planning framework that leverages the concept of restrictive potential fields as cost maps to forge demonstrably safe routes. The algorithm achieves it by segmenting the potential field into a hierarchy of cells, each with a designated restriction zone determined by the obstacles proximity. While the primary impetus behind Larp is to enhance the safety of aerial pathways for Unmanned Aerial Vehicles (UAVs), its utility extends to a wide array of path planning scenarios. Comparative analyses with both established and contemporary potential field-based methods reveal Larp's proficiency in maintaining a safe distance from restrictions and its adeptness in circumventing local minima.

## I. INTRODUCTION

As we look to the future, the role of aerial cargo delivery is expected to become central in the domain of urban goods transportation. Given its growing importance, the development of solutions that are both scalable and verifiably safe is crucial [1]–[3]. Safety is a paramount concern, and routing solutions are integral to this aspect. The flight paths chosen for unmanned aerial vehicles (UAVs) significantly influence the potential for aerial incidents. Consequently, a route's function now extends beyond mere connectivity from origin to destination; it must also encompass considerations for safety.

This paper introduces a path planning framework tailored for restrictive routing within potential fields. It decomposes a potential field into multi-scale cells with an estimated maximum potential for each region and utilizes graph path planning algorithms to generate routes that overcome several of the issues with traditional artificial potential field methods. Although, initially conceived to bolster the safety and scalability of UAV-operated aerial cargo transport within urban air mobility (UAM), the algorithm's utility extends beyond this scope. It is versatile enough to be implemented in any setting that aligns with the potential field standard to be discussed [4].

### A. Background

A variety of distinct and diverse routing approaches have been proposed for the path planning of UAVs and similar vehicles in complex environments [5]. Two prominent

categories are sampling-based and node-based approaches, which involve sampling or deconstructing the environment into networks of nodes or cells for navigation, respectively. Any sector containing an obstacle is excluded from consideration, and the remaining space is searched for optimal routing. Node-based and some sampling-based approaches often employ established graph path planning algorithms to determine routes after decomposing the feasible space. Notable algorithms in these categories include rapidly-exploring random trees (RTTs), artificial potential fields (APFs), A\*, and their variants [6]–[12].

Another major category gaining popularity is mathematical model-based approaches. These methods formulate and apply mathematical expressions to determine optimal routes either through optimization or by solving numerical equations. A prominent approach in this category is mixed-integer linear programming (MILP) [13], [14].

Bio-inspired algorithms, as the name suggests, leverage intrinsic properties found in nature to design optimal routes. Ant colony optimization (ACO) and particle swarm optimization (PSO) have become standard algorithms within this category [15]–[17].

Reinforcement learning-based algorithms are a recent class of algorithms that have emerged from advancements in the field of machine learning. These methods fundamentally optimize a model for sequential decision-making in route search [18]–[20]. A subset of these methods has also been trained to work with potential fields for path planning [20]. However, due to the 'black box' nature of data-driven models and their non-deterministic output, machine learning models are not considered for comparison in this research. Routes for cargo UAVs must be reproducible, scalable, and verifiable for practical application.

### B. Contributions

A significant portion of the works reviewed focus on grid-based environments, which may not accurately reflect real-world situations. Moreover, only a handful of these works actively incorporate variable proximity to restrictions as part of their route search. Our work stands out as one of the few to considers the safety of the generated routes and their potential to violate restrictions.

Akin to our work, [12], [21] explore the application of potential fields for path planning, with [12] employing them specifically to quantify safety. These studies also utilize graph-based algorithms such as A\* to navigate around local minima, a well-known issue associated with APFs methods. However, the methodology of [12] is confined to grid-based

This research has been financially supported by NASA University Leadership Initiative for the project "Autonomous Aerial Cargo Operations at Scale".

Josue N. Rivera and Dengfeng Sun are with School of Aeronautics and Astronautics, Purdue University, 701 W Stadium Ave, West Lafayette, IN 47907 {river264, dsun}@purdue.edu

environments, and [21] primarily applies A\* within a grid context to overcome local minima, which may lead to routes that are not optimized for distance.

Our work expands upon these concepts by considering both continuous and complex spaces within a unified potential field framework. We examine dynamic proximity to obstacles using multi-resolution cells and assign a safety guideline to routes in both complex and non-complex environments through the concept of potential for restriction violation.

## II. PRELIMINARIES

### A. Restrictive Routing Potential Fields

In [4], we explore the problem of last-mile UAVs air management and aerial cargo delivery in urban environments, and introduce a standard for restrictive routing based on a repulsive artificial potential field. Assuming a constant operating altitude, physical and virtual restrictions are designated as areas of high potential that diminishes the further an UAV (or agent) is from an obstacle; a behavior dictated by their repulsion matrix.

The standardization facilitates a uniform approach to potential field construction, enabling consistent replication and analysis across different routing algorithms. By leveraging the structured nature of the field, such algorithms can efficiently navigate through complex environments utilizing a common standard, avoiding obstacles, and minimizing the risk of restriction violations. The potential field delineated herein is henceforth denoted as a ‘restrictive routing potential field’.

### B. Standardized Potential Field Units

Under the proposed standard, a restrictive routing potential field is comprised of multiple building block units, each corresponding to a distinct type of restriction. Upon examining their definitions, a set of intrinsic properties emerges: a repulsion vector  $\bar{x}$ , a scaled squared distance  $\tilde{d}^2(x)$ , and a potential evaluation  $\sigma(x)$ . The repulsion vector  $\bar{x}$  encodes the direction and proximity from the restricted areas. The scaled squared distance  $\tilde{d}^2(x)$  reflects the scaled proximity to a point  $x$ , modulated by the unit’s repulsion matrix  $A$ . Finally, the potential  $\sigma(x)$  denotes the field’s influence at point  $x$ , effectively reflecting the potential for restriction violation.

The repulsion vectors for the fundamental units and collection of them are detailed in Table I. Fig. 1 illustrate the repulsion vectors for an arbitrary set of obstacles with respect to an arbitrary point. The magnitude of each vector indicates proximity to the obstacle and the direction provides a guide towards moving away from it.

**Definition 1** (Squared Distance to a Potential Field Unit). *A proxy to the squared distance to a potential field unit  $d^2(x)$  is defined as:*

$$d^2(x) = \bar{x}(x)^T \bar{x}(x),$$

where  $\bar{x}(x)$  is the repulsion vector detailed in Table I and  $x$  is an evaluated point. For a collective of units,  $d^2(x)$  is the smallest squared distance among all sub-units.

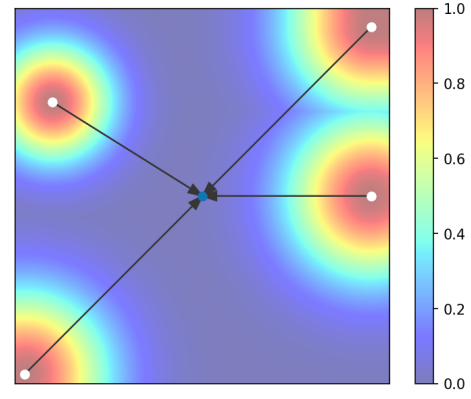


Fig. 1: Illustration of the repulsion vectors with respect to a location.

**Definition 2** (Scaled Squared Distance to a Potential Field Unit). *The scaled squared distance to a potential field unit  $\tilde{d}^2(x)$  is defined as:*

$$\tilde{d}^2(x) = \bar{x}(x)^T A^{-1} \bar{x}(x),$$

where  $\bar{x}(x)$  is again the repulsion vector from Table I,  $A$  is the positive definite repulsion matrix of the unit, and  $x$  is an evaluated point. In the case of a collection of units,  $\tilde{d}^2(x)$  is the minimum of the scaled squared distances with respect to its sub-units.

**Definition 3** (Potential of an Unit). *The potential of a unit  $\sigma(x)$  is defined as the exponential of the scaled squared distance to the unit:*

$$\sigma(x) = \exp\left(\tilde{d}^2(x)\right),$$

where  $\tilde{d}^2(x)$  is the scaled squared distance, and  $x$  is an evaluated point.

## III. METHODOLOGY

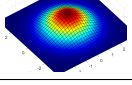
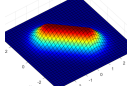
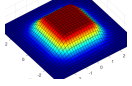
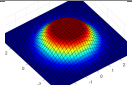
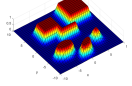
Given the properties of the standardized potential field, we introduce Larp (Last-mile restrictive path planning) as a routing framework for safe path planning. It consists of three core stages: first, a core algorithm that decomposes a field into distinct multi-scale cells; secondly, the formation of a routing network using the cells and an adjacency detection algorithm; lastly, it traverses the graph to determine a suitable route. The stages can be observed in Fig. 2.

Note that an official implementation of Larp can also be found on our Github repository at <https://github.com/wzjoriv/Larp>.

### A. Multi-Scale Cell Decomposition

Drawing inspiration from adaptive quad tree cell decomposition, the first and main phase consists of partitioning a potential field into a multitude of cells, each varying in size. These cells are then correlated with their respective potential for infringing nearby restrictions. The stratagem for cell subdivision is calibrated, ensuring that cells proximal to obstacles are proportionately smaller, thereby augmenting

TABLE I: Restrictive Routing Potential Field Units

Unit	Parameters	Repulsion vector $\bar{x}(x)$	Field
Point	Location $\hat{x}$ Repulsion matrix A	$\bar{x}_p(x) = x - \hat{x}$	
Line	Line start $\hat{x}_1$ Line end $\hat{x}_2$ Repulsion matrix A	$\rho(x) = \frac{(\hat{x}_2 - \hat{x}_1) \cdot (x - \hat{x}_1)}{\ \hat{x}_2 - \hat{x}_1\ ^2}$ $\bar{x}_l(x) = x - \hat{x}_1 + \text{clamp}(\rho(x), 0, 1)(\hat{x}_2 - \hat{x}_1)$	
Rectangle	Corner $\hat{x}_1$ Opposite corner $\hat{x}_2$ Repulsion matrix A	$g(x) = \frac{1}{2}( x - \hat{x}_1  +  x - \hat{x}_2  -  \hat{x}_1 - \hat{x}_2 )$ $\bar{x}_r(x) = \text{sign}(x - \hat{x}_1) \odot g(x)$	
Ellipse	Location $\hat{x}$ Repulsion matrix A Ellipse shape matrix B	$\bar{x}_e(x) = \max\left(1 - \frac{1}{\ B^{-1}(x - \hat{x})\ }, 0\right)(x - \hat{x})$	
Collection	Parameters of the sub units	Repulsion vector $\bar{x}(x)$ of sub unit with smallest scaled squared distance $\tilde{d}^2(x)$	

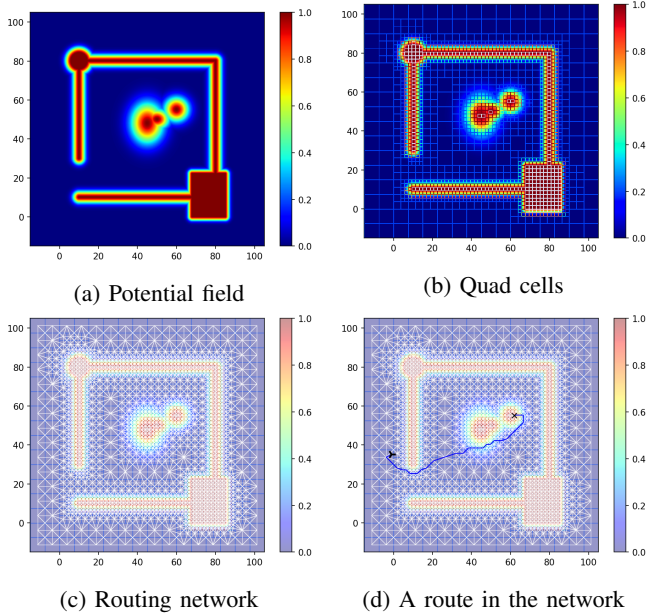


Fig. 2: Stages of Larp for a walled room scene

routing precision and safety. Fig. 2b illustrates this decomposition for a walled room scene. The methodology behind cell decomposition is expounded in Algorithms 1 and 2.

*1) Cells Quad Tree Structure:* Algorithm 1 consists of a recursively subdividing a field into quadrants (i.e., quad or cell) and assigning a restriction zone based on the area potential for violating a restriction. This forms a tree structure with quad cells as node. The tree allows for quick search of any area and the restrictions in it. An example of the quad tree structure is presented in Fig. 3 for a simple field. Initially, at the start of the algorithm, an empty node is initialize for the current observed quadrant. Then, via Algorithm 2, and

the smallest (i.e., closest) zone is assigned from a list of upper limit potentials. Once a zone has been assigned, it is determined whether the subdivision should stop or continues. It stops if we have assigned the further zone allowed or the minimum desired cell size has been reached. After that, we remove any obstacle from consideration that is too far from the quadrant and subdivide again for each quadrant inside the current sector. The leaves of the generated tree allow us to understand the multi-scale cell decomposition of the field and the individual restriction zone.

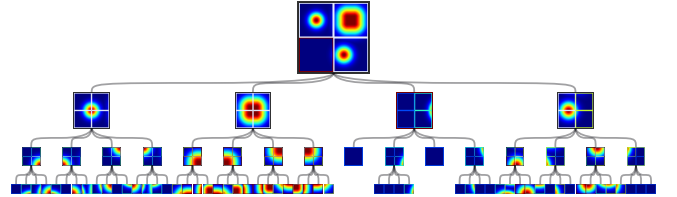


Fig. 3: Quad tree for a simple potential field.

*2) Repulsion Vectors and Potential of an Area:* The heart of the cell decomposition is estimating the potential of any area in the potential field and assigning a restriction zone. This is done by Algorithm 2. By relying on the intrinsic properties of the standardized potential field, an upper limit estimate for the potential to violate restrictions of any cell is analytically determined. Initially, we calculate the square distance of each obstacle unit with respect to the center of a quad. If the distance is less than the radius of the circumscribed circle of the quad, then the obstacle is assigned zone 0 (i.e., an obstacle exists in the area). Trivially, this ensures that if an obstacle is in the area, it is classified as being in zone 0. For the other zones, we must rely on the scaled distance to the obstacles. First, we use the repulsion

---

**Algorithm 1** Larp – Quad Tree Cell Decomposition

---

**Require:** minimum cell size  $n_{min}$ ; maximum cell size  $n_{max}$

```
function BUILD( $x, n, U$ )  
   $quad \leftarrow QuadNode(x, n)$   
   $zones \leftarrow \text{map with default farthest zone}$   
  if  $|U| > 0$  then  
     $zones \leftarrow APPROXOBSTACLESZONES(x, n, U)$   
  end if  
   $quad.zone \leftarrow \min(zones) \triangleright \text{Farthest zone if empty}$   
  if  $n \leq n_{max}$  then  
    if  $n \leq n_{min}$  or  $quad.zone$  is farthest zone then  
      Mark  $quad$  as leaf  
      return  $quad$   
    end if  
  end if  
   $U \leftarrow \{u \in U \mid zones[u] < \text{farthest zone}\}$   
  for each quad  $q$  of a cell do  
     $quad.child[q] \leftarrow BUILD(q.center, n/2, U)$   
  end for  
  return  $quad$   
end function  
 $root \leftarrow BUILD(field.center, field.size, \text{all units in field})$ 
```

---

vector of each obstacle to estimate a location  $c$  of where the obstacle is closest to the area. Then, we sample the potential at this location for each obstacle individually and assign it to a zone based on how close they are to the value 1.0. Each zone assigned is based the potential of each obstacle to be violated by an agent in the area (or indirectly their weighted proximity of the sector to the restriction).

---

**Algorithm 2** Larp – Estimate Potential of a Quad

---

**Require:** Sorted list of boundaries  $bds$  in descending order

```
function APPROXOBSTACLESZONES( $x, n, U$ )  
   $zones \leftarrow \text{map with default farthest zone}$   
  for each unit  $u$  in  $U$  do  
    if  $d_u^2(x) \leq \frac{n^2}{2}$  then  
       $zones[u] \leftarrow 0$   
    end if  
  end for  
  for each unit  $u$  in  $U$  but not already in  $zones$  do  
     $c = x - \frac{n}{\sqrt{2} \|\bar{x}_u(x)\|} \bar{x}_u(x)$   
     $p = \exp\left(\tilde{d}_u^2(c)\right)$   
    Assign  $zones[u]$  into bin given  $bds$  and  $p$   
  end for  
  return  $zones$   
end function
```

---

Fig. 4 illustrates how an area restriction zone can be determined. First, the repulsion vector of each obstacle here is flipped and camped to the magnitude of the diagonal distance to the edge of the quad from its center. In the figure, they are drawn from the center of the area and colored based on the restriction boundary zone assigned. The potential

boundary zones for this example is ticked in the color bar. As the zone for the obstacle to the right of the center is the closest to 1.0, the entire circular area is estimated to have an upper bound of 0.8. As a subset of the area, the quad is also estimated to have an upper bound of 0.8.

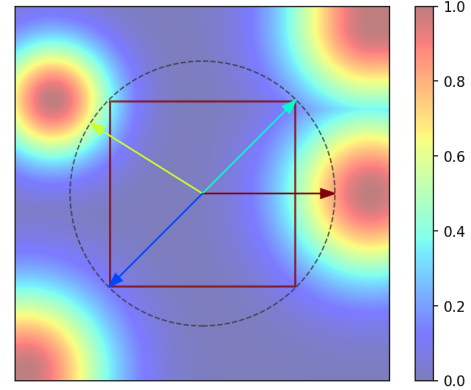


Fig. 4: Estimating the upper bound of an given area in the potential field.

### B. Routing network

To streamline path planning within the designated space, a network graph is constructed subsequent to the potential field's decomposition. The process employs a divide-and-conquer approach to traverse the quad tree, facilitating the identification of neighboring nodes for any given leaf quad node. The intricacies of the field are distilled into a simplified network, where each graph node correlate with a leaf cell and its upper bound potential for the vicinity. Fig. 2c provides a visual representation of this network graph.

In the interest of brevity, we have omitted the detailed adjacency algorithm used to construct the routing network; however, it is available for review in our public repository.

### C. Path Planning

Upon the establishment of the network, the implementation of any graph routing algorithm that simultaneously minimizes route distance and accumulated potential is feasible. For this study, we employ a modified variant of the renowned A\* algorithm, wherein the distance function is redefined as:

$$d(q_a, q_b) = s(q_b) \cdot \|q_a.center - q_b.center\| \quad (1)$$

where  $q_a$  and  $q_b$  denote the quadrant being traversed from and to, respectively;  $s(q)$  represents scale transformation function that modulates the penalty of going to a new sector given its potential upper boundary; and  $q_a.center$  signifies the centroid of cell  $q_a$ . A route generated for the walled room scene is depicted in Fig. 2d. Subsequent to determining a routing solution, line segments are integrated to connect the initial location and the destination with the discovered route within the network.

#### D. Safety Validation

Prior to assessing the safety of a route, it is imperative to define what constitutes a route within a potential field.

**Definition 4** (Route in a Potential Field). *A route  $R$  within a restrictive routing potential field is delineated as a trajectory comprising a line string that interconnects a sequence of points, expressed as:*

$$R_p = \{x_1, x_2, \dots, x_N\}$$

where  $x_i$  signifies a 2D coordinate in a plane, and  $N-1$  represents the count of consecutive line segments that constitute the line string.

With Definition 4 established, several metrics to evaluate the safety of a route can be examined. The primary metric is the cumulative potential under a route's trajectory, calculated as:

$$R_A = \int_R \sigma(x_t) dx_t = \sum_{i=0}^{N-1} \int_{x_i}^{x_{i+1}} \sigma(x_t) dx_t \quad (2)$$

where  $\sigma(\cdot)$  denotes the potential field assessment, and  $\int_{x_i}^{x_{i+1}} \sigma(x_t) dx_t$  encapsulates the line integral from point  $x_i$  to point  $x_{i+1}$ . This metric gauges the aggregate potential for committing a restriction violation by an agent traversing the route, with higher values indicating increased interaction with restricted regions.

Conversely, a route's length as a measure of safety is considered:

$$R_d = \int_R 1 dx_t = \sum_{i=0}^{N-1} \int_{x_i}^{x_{i+1}} 1 dx_t \quad (3)$$

The extended duration of a route implies a prolonged presence within the field, potentially elevating the risk of violation occurrences.

Ultimately, combining these two metrics yields a composite measure that reflects the average engagement with restrictions along a route

$$R_{avg} = \frac{R_A}{R_d} \quad (4)$$

A heightened  $R_{avg}$  value suggests a route's active proximity to restricted areas. Empirical observations indicate that a threshold of 0.35 or below is typically indicative of minimal engagement with restrictions.

## IV. EXPERIMENTS AND RESULTS

### A. Potential field-based path planning algorithms

To assess the efficacy of our algorithm, we have compiled a suite of path planning strategies that leverage potential fields to evaluate proximity to obstacles and violating routing restrictions. Detailed implementations and comparisons of these methods are available in our Github repository at <https://github.com/wzjoriv/path-planning-pf>.

1) *Penalty Method with Gradient Descent (PM)*: The penalty method with gradient descent introduces an attractive force that propels an agent towards a goal, defined as:

$$F_A(x) = \zeta(x_g - x) \quad (5)$$

where  $\zeta$  is a scalar hyper-parameter dictating the strength of the attraction, and  $x_g$  denotes the goal's location. Additionally, a repulsive force emerges from a penalty on the potential field value,

$$F_R(x) = -\eta p'(\sigma(x)) \nabla \sigma(x) \quad (6)$$

where  $\eta$  is a scalar hyper-parameter governing the repulsion,  $p'(\cdot)$  is the derivative of the penalty function, and  $\nabla \sigma(x)$  represents the gradient of the potential field under discussion.

Combining these two forces forms a traversal strategy that steers the agent towards the goal, articulated as:

$$x_{i+1} = x_i + \gamma \frac{F_A(x_i) + F_B(x_i)}{\|F_A(x_i) + F_B(x_i)\|} \quad (7)$$

where  $\gamma$  signifies the step size, and  $x_0$  is the agent's initial location. To circumvent local minima near the goal, our experiments introduce a heuristic: if  $\|x_N - x_g\| \leq 2.5$ , a direct line segment to the goal  $x_g$  is appended to the route's  $R_p$ .

2) *Artificial Potential Field (APF, APF(\*))*: The classical APF method supplants the gradient-based approach with a traditional repulsive force as delineated in [10], [22]. Within the scope of the problems addressed, this repulsive force is articulated by:

$$F_R(x) = \begin{cases} \eta \left( \frac{1}{d(x)} - \frac{1}{d_o} \right) \frac{1}{d^2(x)} \bar{x}(x), & \text{if } d(x) \leq d_o \\ 0, & \text{otherwise} \end{cases} \quad (8)$$

where  $d(x) = \sqrt{d^2(x)}$ ,  $d_o$  is the threshold distance at which the repulsive force becomes active, and  $\bar{x}(x)$  is the repulsion vector from the nearest obstacle.

Subsequent enhancements to the APF methodology, not originally included but recommended for improved efficacy, propose an alternative attraction force [22]:

$$F_A(x) = \begin{cases} \zeta(x_g - x), & \text{if } \|x - x_g\| \leq d_g \\ \zeta d_g \frac{x_g - x}{\|x - x_g\|}, & \text{otherwise} \end{cases} \quad (9)$$

where  $d_g$  is the critical distance beyond which the attraction force adopts a quadratic profile to ensure a smooth convergence to the target.

For the APF method, a variant denoted as APF (\*) is also implemented for which square distance function  $d^2(x)$  is substituted with its scaled counterpart  $\tilde{d}^2(x)$ .

3) *Modified Artificial Potential Field (M-APF)*: M-APF, an advanced iteration of APF introduced by [8], [23], innovates upon the conventional repulsion force to mitigate the issue of local minima. The reformulated force is expressed



by:

$$F_{R1}(x) = \eta \left( \frac{1}{d(x)} - \frac{1}{d_o} \right) \|x - x_g\|^{m-3}$$

$$F_{R2}(x) = \eta m \left( \frac{1}{d(x)} - \frac{1}{d_o} \right)^2 \|x - x_g\|^m \quad (10)$$

$$F_R(x) = \begin{cases} F_{R1}(x) + F_{R2}(x) \frac{\bar{x}(x)}{\|\bar{x}(x)\|}, & \text{if } d(x) \leq d_o \\ 0, & \text{otherwise} \end{cases}$$

where  $m$  is a positive scalar hyper-parameter that modulates the repulsion force's sensitivity to the agent's proximity to the goal.

### B. Results: Routes in a small room

In evaluating these algorithms, we explored three distinct scenarios of path planning in a small room.

1) *Scenario 1 (Unobstructed Path)*: The first scenario considers a straightforward path planning task where the objective is to travel towards an unobstructed target. Although there are no significant obstacles present, this scenario serves to accentuate the subtle differences between the algorithms. As shown in Table II and Fig. 5, even in an ideal situation where no obstacles impede the path, Larp—placing a premium on safety—may yield routes that are marginally longer if it results in a lower overall potential energy.

TABLE II: Performance metrics for Scenario 1. All algorithms successfully reach the goal. Larp generates a slightly longer path due to its conservative movements and emphasis on safety. A  $\checkmark$  under 'Goal Found' indicates  $\|x_N - x_g\|^2 \leq 2.5$  where  $x_N$  is the final position of a route.

Algorithm	Goal Found	Route Distance	Route Area	Average Potential	Highest Potential
PM	$\checkmark$	62.04	0.4006	0.0065	0.0619
APF	$\checkmark$	62.06	0.3863	0.0062	0.0594
APF (*)	$\checkmark$	<b>62.02</b>	0.4020	0.0065	0.0622
M-APF	$\checkmark$	<b>62.02</b>	0.4020	0.0065	0.0622
Larp (Our)	$\checkmark$	62.9181	<b>0.1082</b>	<b>0.0017</b>	<b>0.0084</b>

2) *Scenario 2 (Obstructed Path and Near-Obstacle Goal)*: This scenario examines the algorithms' performance when an agent must navigate around an obstacle and when the target is in close proximity to one. The results are presented in Table III and Fig. 6. When obstacles are introduced along the route, both PM and APF struggle to maintain a safe distance from the constraints, resulting in higher peak potential values. PM's dependence on gradients and penalties hinders its ability to significantly deviate from the obstacle's path. APF's higher potential can be attributed to its focus on immediate obstacle proximity rather than the overall potential for obstacle avoidance; however, it also contributes to its shorter route distance. Among all the methods evaluated, Larp consistently produced safer routes, albeit at the expense of increased distance. Nevertheless, Larp's route lengths remain competitive, particularly when compared to methods such as APF (\*) and M-APF.

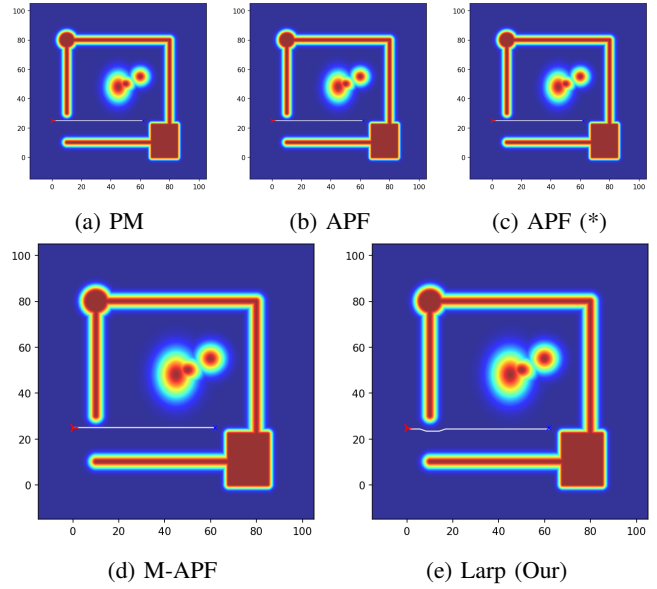


Fig. 5: Comparison of routes in Scenario 1, featuring an unobstructed path. The red marker indicates the initial location of the agent.

TABLE III: Performance metrics for Scenario 2. The highest potential energy values for APF (\*), M-APF, and Larp reflect the goal's proximity to obstacles.

Algorithm	Goal Found	Route Distance	Route Area	Average Potential	Highest Potential
PM	$\checkmark$	79.188	23.1432	0.2923	0.9011
APF	$\checkmark$	<b>77.2863</b>	23.011	0.2977	0.9220
APF (*)	$\checkmark$	87.8328	29.3081	0.3337	<b>0.8948</b>
M-APF	$\checkmark$	80.8579	21.0194	0.26	<b>0.8948</b>
Larp (Our)	$\checkmark$	83.8675	<b>15.8687</b>	<b>0.1892</b>	<b>0.8948</b>

3) *Scenario 3 (Walled-Off Path)*: The final scenario investigates the behavior of the methods when the direct route to a target is obstructed by a wall. As depicted in Table IV and Fig. 7, all methods, except for Larp, fail to reach the destination. When confronted with non-circular restrictions, both penalty-based and force-based methods may struggle to overcome the local minima created by the opposing forces of attraction and repulsion from the obstacles.

### C. Results: UAV routes in Austin, TX

Larp is capable of generating safe city-level routes. To test its capability, UAV routes for Austin, TX were generated using OpenStreetMap buildings data. It is assumed that all buildings are tall enough to interfere with UAVs travel, while anything outside of the area does not. Fig. 8 and 9 explore two similar but distinct scenarios involving urban air mobility.

In Fig. 8, travel within an urban environment is explored, specifically focusing on safe route generation inside a dense neighborhood. As shown, Larp has the ability to generate routes that maintain a safe distance from building boundaries (colored deep red with a potential of 1) wherever possible. It only enters a building's airspace when required to perform

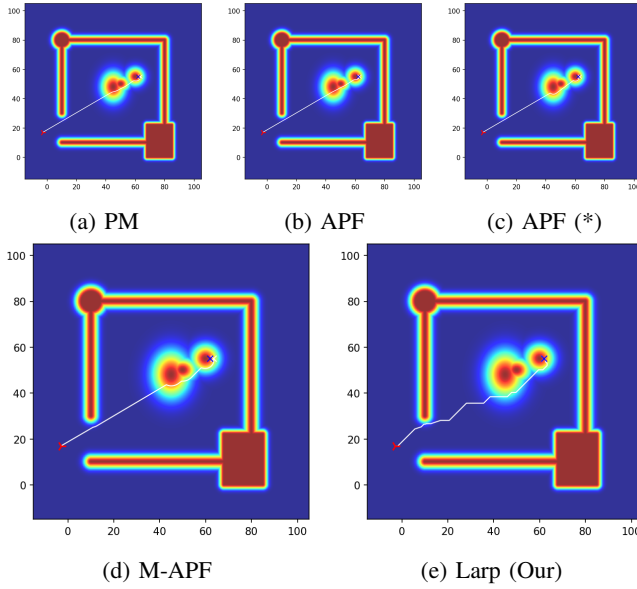


Fig. 6: Scenario 2 of an obstructed path and near-obstacle goal (routes comparison)

TABLE IV: Performance metrics for Scenario 3. Except for Larp, all other methods are unable to reach the target; therefore, their performance measurements are not valid for comparison but provide insight into their behavior. In this table, an  $\times$  under 'Goal Found' indicates  $\|x_N - x_g\|^2 > 2.5$

Algorithm	Goal Found	Route Distance	Route Area	Average Potential	Highest Potential
PM	$\times$	33.32	18.6015	0.5583	0.9529
APF	$\times$	42.83	26.3972	0.6163	0.9075
APF (*)	$\times$	80.37	53.9457	0.6712	0.8075
M-APF	$\times$	38.57	1.8687	0.0485	0.0674
Larp (Our)	$\checkmark$	<b>163.8382</b>	<b>14.8769</b>	<b>0.0908</b>	<b>0.3453</b>

the delivery. Additionally, routes can adapt to crevices created by a number of buildings. Note that the scale of the axes is in meters, and the policy for proximity to buildings can be adjusted during path planning by the penalty function. For this demo, we have chosen to set an upper potential for restriction violation at 0.2, only getting closer when necessary without violating boundary restrictions.

Fig. 9 presents the results when the algorithm is expanded to a larger scale, including rural or unobstructed areas. In this scenario, the surrounding areas of Austin transition from an urban sector to an unobstructed space. As observed, Larp generates coarse paths when away from buildings and granular paths when near them. The coarse paths allow for easier straight flights, which are convenient for long-distance travel without drastic maneuvering. When near a building, the granular, smoother, and more precise routes allow for safer navigation around the buildings. For the demo, and as illustrated, the routes for UAVs avoid buildings wherever possible. However, to ensure deliveries to buildings, we have opted to allow entrance into a building's airspace if necessary for delivery, as seen in the previous scenario.

The source code to generate the routes near

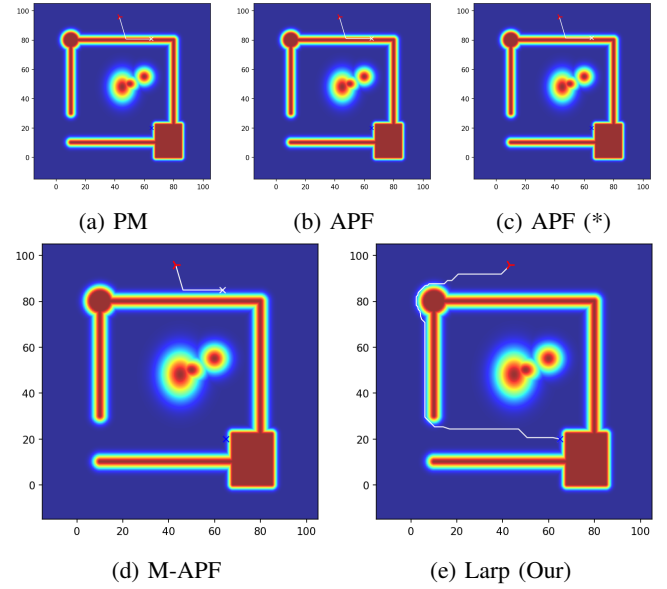


Fig. 7: Routes comparison for Scenario 3, featuring a walled-off path.

Austin, TX can be found on our Github repository at <https://github.com/wzjoriv/Larp>. A GeoJSON file of the city's or neighborhood's buildings is needed to run it. It can be obtained via OpenStreetMap or similar map providers.

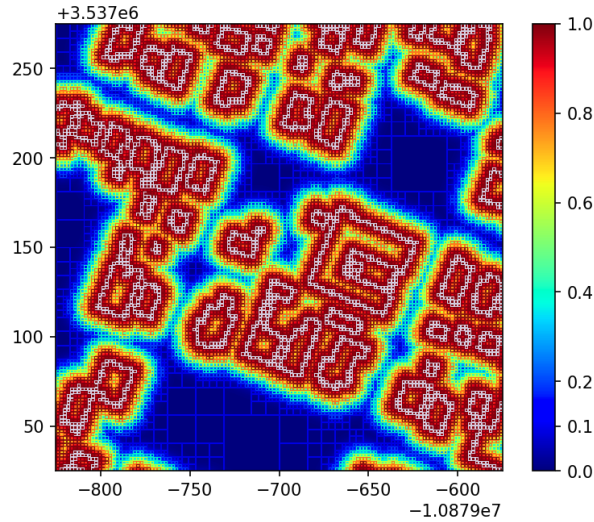
## V. CONCLUSION

In this work, we have presented Larp, an innovative path planning framework tailored for restrictive routing within potential fields. Demonstrating superior results, Larp outperforms both traditional and contemporary potential field-based methodologies by reliably crafting safer routes that diminish the risk of restriction violations, all while preserving comparative efficiency in terms of travel distance. This is achieved through an initial segmentation of the potential field into multi-scale cells, with each cell's restriction zone determined by its proximity to nearby obstacles. For transparency and to facilitate further research, the source code for an official implementation of Larp has been made publicly accessible.

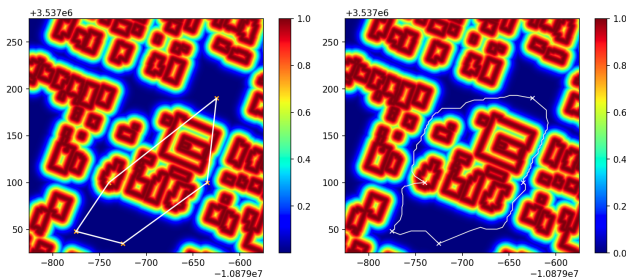
While Larp marks an advancement in route safety, opportunities for improvement remain. The framework's quad cell decomposition approach and zone classification system are poised for further optimization. The influence of a cell's dimensions and positioning on the placement of subsequent cells is a critical factor in the pursuit of optimally short and safe routes. Moreover, the current method of zone classification, which relies on an proxy scaled distance to a cell's periphery to gauge the highest potential across the region, may estimate an higher potential for a region that what it is. Future endeavors will concentrate on refining these elements and developing a dynamic and scalable system capable of storing and updating cells in real-time to adapt to evolving restrictions for unmanned aircraft system traffic management (UTM).

## REFERENCES

- [1] Rakesh Shrestha, Inseon Oh, and Shiho Kim. A survey on operation concept, advancements, and challenging issues of urban air traffic management. *Frontiers in Future Transportation*, 2:1, 2021.
- [2] Khaled Telli, Okba Kraa, Yassine Himeur, Abdelmalik Ouamane, Mohamed Boumehraz, Shadi Atalla, and Wathiq Mansoor. A comprehensive review of recent research trends on unmanned aerial vehicles (uavs). *Systems*, 11(8):400, 2023.
- [3] Bhawesh Sah, Rohit Gupta, and Dana Bani-Hani. Analysis of barriers to implement drone logistics. *International Journal of Logistics Research and Applications*, 24(6):531–550, 2021.
- [4] Josue N Rivera and Dengfeng Sun. Air traffic management for collaborative routing of unmanned aerial vehicles via potential fields. In *2024 International Conference on Research in Air Transportation (ICRAT)*, 2024.
- [5] Michael Jones, Soufiene Djahel, and Kristopher Welsh. Path-planning for unmanned aerial vehicles with environment complexity considerations: A survey. *ACM Computing Surveys*, 55(11):1–39, 2023.
- [6] Pengcheng Wu, Junfei Xie, and Jun Chen. Safe path planning for unmanned aerial vehicle under location uncertainty. In *2020 IEEE 16th International Conference on Control & Automation (ICCA)*, pages 342–347. IEEE, 2020.
- [7] Tai Huang, Kuangang Fan, Wen Sun, Weichao Li, and Haoqi Guo. Potential-field-rrt: A path-planning algorithm for uavs based on potential-field-oriented greedy strategy to extend random tree. *Drones*, 7(5):331, 2023.
- [8] Seyyed Mohammad Hosseini Rostami, Arun Kumar Sangaiah, Jin Wang, and Xiaozhu Liu. Obstacle avoidance of mobile robots using modified artificial potential field algorithm. *EURASIP Journal on Wireless Communications and Networking*, 2019(1):1–19, 2019.
- [9] Chunyu Ju, Qinghua Luo, and Xiaozhen Yan. Path planning using an improved a-star algorithm. In *2020 11th International Conference on Prognostics and System Health Management (PHM-2020 Jinan)*, pages 23–26. IEEE, 2020.
- [10] Yong K Hwang and Narendra Ahuja. A potential field approach to path planning. *IEEE transactions on robotics and automation*, 8(1):23–32, 1992.
- [11] Jinchao Chen, Mengyuan Li, Zhenyu Yuan, and Qing Gu. An improved a\* algorithm for uav path planning problems. In *2020 IEEE 4th Information Technology, Networking, Electronic and Automation Control Conference (ITNEC)*, volume 1, pages 958–962. IEEE, 2020.
- [12] Jinjun Rao, Chaoyu Xiang, Jinyao Xi, Jinbo Chen, Jingtao Lei, Wojciech Giernacki, and Mei Liu. Path planning for dual uavs cooperative suspension transport based on artificial potential field-a\* algorithm. *Knowledge-Based Systems*, 277:110797, 2023.
- [13] Kaiping Wang, Mingzhu Song, and Meng Li. Cooperative multi-uav conflict avoidance planning in a complex urban environment. *Sustainability*, 13(12):6807, 2021.
- [14] Mohammadreza Radmanesh, Manish Kumar, Alireza Nemati, and Mohammad Sarim. Dynamic optimal uav trajectory planning in the national airspace system via mixed integer linear programming. *Proceedings of the Institution of Mechanical Engineers, Part G: Journal of Aerospace Engineering*, 230(9):1668–1682, 2016.
- [15] Yanli Chen, Guiqiang Bai, Yin Zhan, Xinyu Hu, and Jun Liu. Path planning and obstacle avoiding of the usv based on improved aco-apf hybrid algorithm with adaptive early-warning. *Ieee Access*, 9:40728–40742, 2021.
- [16] Wenbin Hou, Zhihua Xiong, Changsheng Wang, and Howard Chen. Enhanced ant colony algorithm with communication mechanism for mobile robot path planning. *Robotics and Autonomous Systems*, 148:103949, 2022.
- [17] Chenchen Xu, Xiaohan Liao, Huanyin Yue, Xiaoming Deng, and Xiwang Chen. 3-d path-searching for uavs using geographical spatial information. In *IGARSS 2019-2019 IEEE International Geoscience and Remote Sensing Symposium*, pages 947–950. IEEE, 2019.
- [18] Jingzhi Hu, Hongliang Zhang, Lingyang Song, Zhu Han, and H Vincent Poor. Reinforcement learning for a cellular internet of uavs: Protocol design, trajectory control, and resource management. *IEEE Wireless Communications*, 27(1):116–123, 2020.
- [19] Sarthak Bhagat and PB Sujit. Uav target tracking in urban environments using deep reinforcement learning. In *2020 International conference on unmanned aircraft systems (ICUAS)*, pages 694–701. IEEE, 2020.



(a) Cell decomposition of neighborhood.



(b) Initial delivery points. (c) Routes generated by Larp.

Fig. 8: Routes among buildings in downtown Austin, TX.

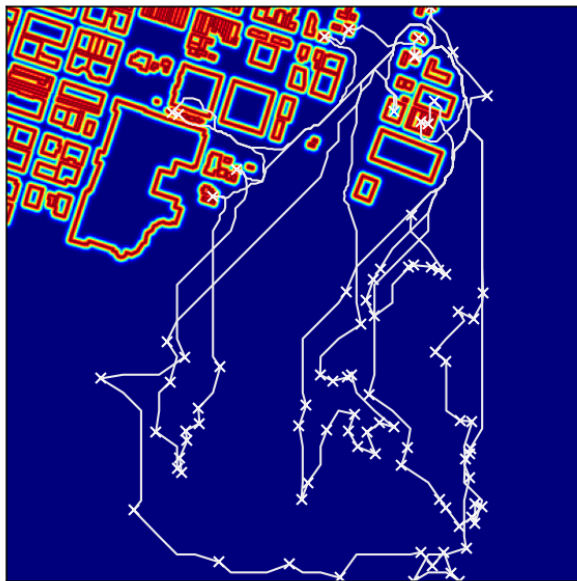


Fig. 9: Routes surrounding Austin, TX.



- [20] Fuchen Kong, Qi Wang, Shang Gao, and Hualong Yu. B-apfdqn: A uav path planning algorithm based on deep q-network and artificial potential field. *IEEE Access*, 2023.
- [21] Ahmed S Abdel-Rahman, Shady Zahran, Basem E Elnaghi, and SF Nafea. Enhanced hybrid path planning algorithm based on apf and a-star. *The International Archives of the Photogrammetry, Remote Sensing and Spatial Information Sciences*, 48:867–873, 2023.
- [22] Howie Choset, Ji Y Lee, G.D. Hager, and Z. Dodds. Lecture notes in robotic motion planning: potential functions, 2010.
- [23] Farid Bounini, Denis Gingras, Herve Pollart, and Dominique Gruyer. Modified artificial potential field method for online path planning applications. In *2017 IEEE Intelligent Vehicles Symposium (IV)*, pages 180–185. IEEE, 2017.